Article

Cell Metabolism

Adult NG2-Glia Are Required for Median Eminence-Mediated Leptin Sensing and Body Weight Control

Graphical Abstract

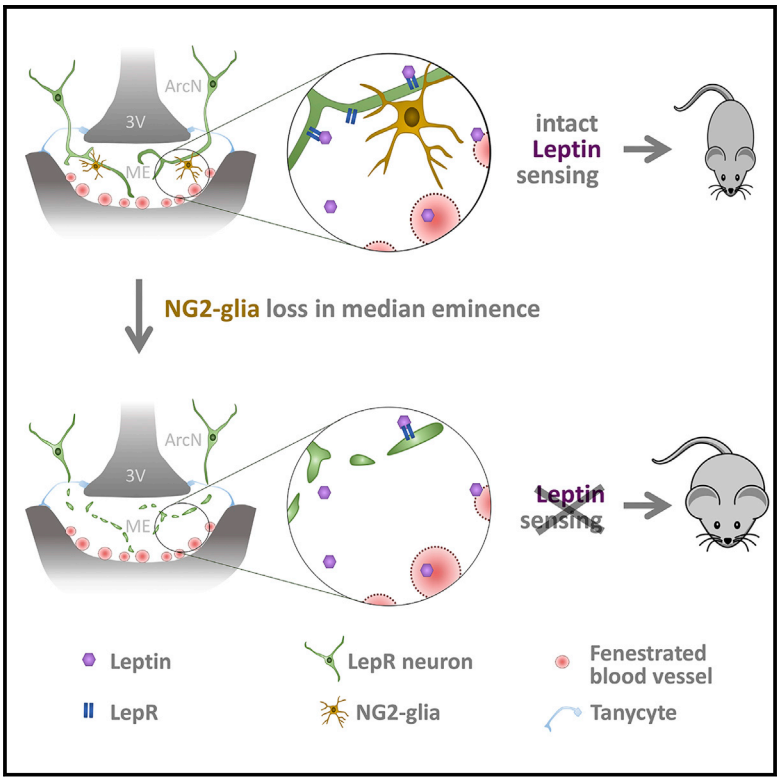

Authors

Tina Djogo, Sarah C. Robins, Sarah Schneider, ..., Thomas Stroh, Leda Dimou, Maia V. Kokoeva

Correspondence

maia.kokoeva@mcgill.ca

In Brief

Djogo et al. show that ablation of NG2-glia, but not microglia, in the median eminence (ME) leads to selective degeneration of LepR dendrites in the arcuate nucleus, causing primary leptin resistance and obesity. These effects are reproduced with ME-directed X-irradiation, possibly explaining the obesity risk associated with cranial radiation therapy.

Highlights

- Pharmacological and genetic ablation of NG2-glia, but not microglia, leads to obesity
- NG2-glial ablation causes LepR processes in the median eminence to degenerate
- Arcuate nucleus LepR neurons lose responsiveness to leptin after NG2-glia ablation
- X-irradiation aimed at the median eminence is sufficient for weight gain induction

Djogo et al., 2016, Cell Metabolism *23*, 797–810
May 10, 2016
http://dx.doi.org/10.1016/j.cmet.2016.04.013

Cell Metabolism
Article

Adult NG2-Glia Are Required for Median Eminence-Mediated Leptin Sensing and Body Weight Control

Tina Djogo,[1,7] Sarah C. Robins,[1,7] Sarah Schneider,[2] Darya Kryzskaya,[1] Xiaohong Liu,[1] Andrew Mingay,[1] Colleen J. Gillon,[1] Joo Hyun Kim,[1] Kai-Florian Storch,[6] Ulrich Boehm,[5] Charles W. Bourque,[4] Thomas Stroh,[3] Leda Dimou,[2] and Maia V. Kokoeva[1,*]

[1]Department of Medicine, McGill University Health Center Research Institute, McGill University, Montreal, QC H4A 3J1, Canada
[2]Physiological Genomics, Institute of Physiology, Ludwig Maximilians University Munich, 80336 Munich, Germany
[3]Department of Neurology and Neurosurgery, Montreal Neurological Institute, McGill University, Montreal, QC H3A 2B4, Canada
[4]Centre for Research in Neuroscience, Montreal General Hospital, McGill University, Montreal, QC H3G 1A4, Canada
[5]Department of Pharmacology and Toxicology, University of Saarland School of Medicine, 66421 Homburg, Germany
[6]Department of Psychiatry, Douglas Mental Health University Institute, McGill University, Montreal, QC H4H 1R3, Canada
[7]Co-first author
*Correspondence: maia.kokoeva@mcgill.ca
http://dx.doi.org/10.1016/j.cmet.2016.04.013

SUMMARY

While leptin is a well-known regulator of body fat mass, it remains unclear how circulating leptin is sensed centrally to maintain energy homeostasis. Here we show that genetic and pharmacological ablation of adult NG2-glia (also known as oligodendrocyte precursors), but not microglia, leads to primary leptin resistance and obesity in mice. We reveal that NG2-glia contact the dendritic processes of arcuate nucleus leptin receptor (LepR) neurons in the median eminence (ME) and that these processes degenerate upon NG2-glia elimination, which explains the consequential attenuation of these neurons' molecular and electrical responses to leptin. Our data therefore indicate that LepR dendrites in the ME represent the principal conduits of leptin's anorexigenic action and that NG2-glia are essential for their maintenance. Given that ME-directed X-irradiation confirmed the pharmacological and genetically mediated ablation effects on body weight, our findings provide a rationale for the known obesity risk associated with cranial radiation therapy.

INTRODUCTION

While much knowledge has been accumulated about the architecture and function of the hypothalamic neurocircuits that control energy balance (Morton et al., 2014), we still know very little about if and how glial cells contribute to the function of these circuits (Balland et al., 2014; Gao et al., 2014; García-Cáceres et al., 2013; Lee et al., 2012; Thaler et al., 2012).

We have shown previously that new cells are constitutively born in the adult hypothalamus (Kokoeva et al., 2005, 2007), including its mediobasal portion, and that the majority of proliferating cells in this brain area are NG2-glia (Robins et al., 2013b, 2013c). NG2-glia represent a major glia cell class known for their role as precursors to oligodendrocytes (Dimou and Gallo, 2015). Despite their dense presence throughout the CNS, including the hypothalamus, their physiological significance in the adult brain has only recently begun to be explored. White matter NG2-glia have been shown to contribute to myelination even post-development (Young et al., 2013), and this myelination improves motor skill learning (McKenzie et al., 2014). NG2-glia receive synaptic input from neurons (Bergles et al., 2000; De Biase et al., 2010), and optogenetic stimulation of premotor cortex neurons not only promotes NG2-glia proliferation, oligodendrogenesis, and myelination, but also leads to improved motor function (Gibson et al., 2014). Interestingly, this glia class exhibits a profound potency to regenerate in the adult brain (Hughes et al., 2013; Irvine and Blakemore, 2007; Robins et al., 2013c). Even when NG2-glia are acutely eliminated from large portions of the periventricular parenchyma upon intracerebroventricular (i.c.v.) infusion of the mitotic blocker cytosine-β-D-arabinofuranoside (AraC), NG2-glia coverage is fully restored within weeks following their ablation (Robins et al., 2013c). Mitotic blocker-mediated NG2-glia cell death is thought to prompt cell division in neighboring, previously mitotically quiescent NG2-glia, which then in turn become vulnerable to AraC (Robins et al., 2013c). This knockon effect seems to be the ultimate cause of the widespread and complete elimination of periventricular NG2-glia upon i.c.v. AraC infusion, despite the fact that in the hypothalamus only 10% of the NG2-glia population is typically mitotically active during the time span of the infusion period (Robins et al., 2013c; Figures 1A–1D).

One of the central sites of energy balance regulation is the arcuate nucleus (ArcN) located at the base of the mediobasal hypothalamus (Williams and Elmquist, 2012). This nucleus is ventrally abutted by the median eminence (ME), a structure that is partitioned from the brain parenchyma by tanycyte processes and that contains fenestrated capillaries, a hallmark of circumventricular organs (Rodríguez et al., 2010). While there is strong evidence that LepR neurons residing in the ArcN and other hypothalamic sites are crucial for body weight control (Vong et al., 2011), it is still unclear how the adipocyte-derived, anorexigenic

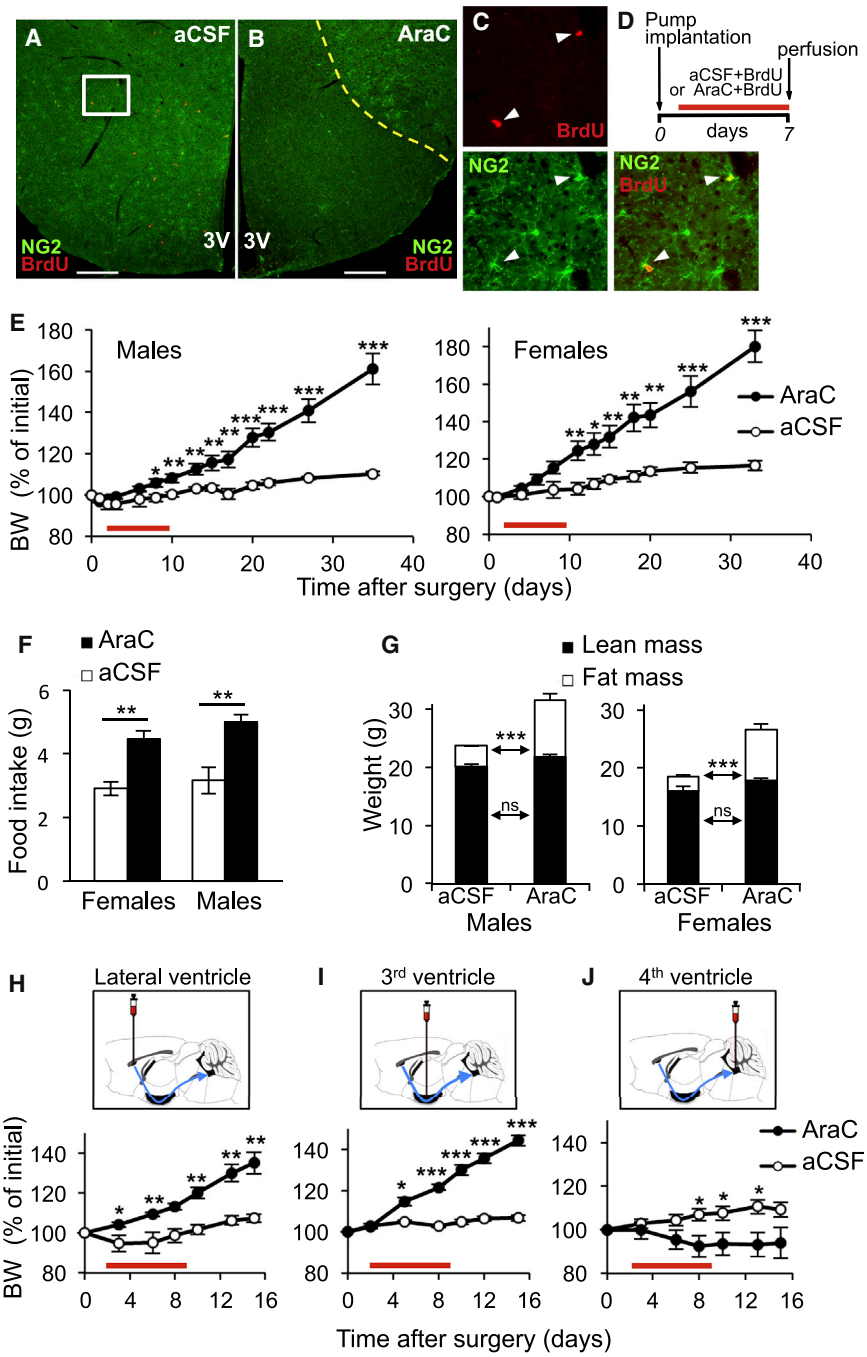

Figure 1. Obesity Induction by Ventricular Mitotic Blocker Infusion

(A–D) Immunodetection of NG2 and the proliferation marker BrdU in the hypothalamus following 1 week of i.c.v. aCSF + BrdU (A) or AraC + BrdU (B) infusion. Yellow dotted line in (B) shows the approximate boundary of NG2-glial ablation. Boxed area in (A) is shown enlarged in (C). (D) Treatment regimen is shown. 3V, third ventricle. Scale bars, 200 μm.

(E) Body weight (BW) changes in response to i.c.v. AraC in male and female mice (n = 5–12). Red bar indicates infusion period.

(F) Daily food intake is shown in male and female mice averaged across days 8–11 post i.c.v. infusion onset (n = 5–8).

(G) Body composition of male and female mice 25 days post i.c.v. infusion onset is shown (n = 5–10).

(H–J) Body weight changes in response to AraC infusion into the lateral (H, n = 5–12), third (I, n = 5–8), or fourth (J, n = 5–7) ventricle compared to aCSF controls (*p < 0.05, **p < 0.01, and ***p < 0.001, unpaired t test; mean ± SEM).

See also Figures S1 and S2.

Here we provide the first functional evidence that central energy balance control chiefly relies on LepR neuronal processes within the ME and that NG2-glia are required for their maintenance, thereby enabling effective leptin sensing by the CNS.

RESULTS

Central Mitotic Blocker Infusion Results in an Obese Phenotype

The i.c.v. infusion of the mitotic blocker AraC in mice resulted in widespread and comprehensive ablation of NG2-glia in the periventricular parenchyma, including the hypothalamus (Figures 1A–1D), within 1 week. Concomitantly, AraC infusion led to a profound and sustained increase in food intake and body weight in both male and female mice (Figures 1E and 1F). The change in food consumption was observable as early as 3 days after the initiation of AraC infusion, and food intake was selectively increased during the light period (Figures S1A and S1B). The latter finding is reminiscent of rodents lacking leptin or its receptor globally, which show a profound increase in food intake that is most prominent during the light period (Becker and Grinker, 1977; Ho and Chin, 1988). AraC-infused mice showed a decline in daily locomotor activity, specifically at night, which reached significance only in females (Figures S1C–S1E). Given the apparent reduction of the day:night difference in food intake and activity, we examined master circadian pacemaker properties in AraC-infused mice by monitoring wheel-running activity

hormone leptin is sensed by the mediobasal feeding circuits (Münzberg and Morrison, 2015). The finding that intraperitoneal-injected, radio-labeled leptin specifically accumulates in the ME (Banks et al., 1996) indicates that this circumventricular organ may play an important role in leptin sensing. Indeed, it has been suggested that leptin exits the fenestrated capillaries of the ME via passive diffusion and that the hormone is then detected by LepR neuronal processes of the ArcN that reach into the ME (Faouzi et al., 2007). However, it also has been proposed that leptin is actively transported across the blood brain barrier (Banks et al., 1996; Golden et al., 1997).

under constant dark conditions (Figures S1F–S1J). We did not detect any abnormalities in circadian period (Figure S1I) or amplitude (Figure S1J), suggesting that rhythm generation by the master clock of the suprachiasmatic nucleus is not affected by periventricular NG2-glia ablation. Consistent with an obese phenotype, the AraC-induced weight gain was associated with a selective increase in body fat mass (Figure 1G).

The Third Ventricular Parenchyma Mediates the Obesogenic Effect of Mitotic Blockade

To identify the periventricular brain site that mediates the AraC effect on body weight, we aimed to regionally restrict mitotic blocker action by infusing AraC at different sites within the ventricular system (Figure S2M). As predicted by the direction of the cerebrospinal fluid (CSF) flow, infusing AraC into the lateral ventricle was found to profoundly ablate NG2 cells not only at the infusion site but also in the parenchyma surrounding the third and fourth ventricles (compare Figures S2A–S2C with S2D–S2F). NG2-glia in the lateral ventricular parenchyma were, however, spared when AraC was directly infused into the third ventricle (Figures S2G–S2I), as were the lateral and third ventricular parenchyma upon infusion into the fourth ventricle (Figures S2J–S2L).

Having established that site-specific AraC infusion corresponded to site-specific ablation of NG2-glia, we next assessed energy homeostasis in such treated animals. Mice that were AraC infused into the third ventricle showed increases in food intake (not shown) and weight gain comparable to mice that received AraC via the lateral ventricle (Figures 1H and 1I), whereas infusion into the fourth ventricle led to a slight and only transient weight decrease (Figure 1J). These results suggest that AraC's obesogenic effect is mediated via the region surrounding the third ventricle, i.e., the hypothalamus.

Microglia Ablation Does Not Increase Body Weight

Although proliferating NG2-glia make up more than 80% of the dividing cells in the adult hypothalamus (Robins et al., 2013c), it is important to consider whether AraC can affect other cell types in the CNS. We previously concluded that the number and morphology of both neurons and astrocytes were not altered by AraC infusion, which is consistent with their status as postmitotic cells (Robins et al., 2013c). We did, however, observe a slight depopulation of microglia, which was temporary and affected a much smaller area (Robins et al., 2013c). To test if ablation of microglia, which represent the second largest group of dividing cells in the hypothalamus and the ME (Figures S3A–S3C), alternatively accounts for the obese phenotype, we treated animals with PLX3397, a colony-stimulating factor 1 receptor (CSF1R) inhibitor. In the adult brain, CSF1R is exclusively expressed by microglia, and, when PLX3397 is provided in the diet, it leads to selective and comprehensive ablation of microglia from the mouse brain (Elmore et al., 2014). Indeed, when adult C57BL/6J mice were switched to PLX3397-containing chow, we observed an almost complete elimination of microglia throughout the hypothalamus, while NG2-glia numbers remained unaffected (Figures 2A–2C). Importantly, the treatment had no effect on body weights (Figure 2D), and body weights continued to be indistinguishable between the groups after a return to regular chow (Figure 2D, arrow), which is known to result in the restoration of microglia coverage (Elmore et al., 2014).

Genetic Ablation of Proliferating NG2-Glia Leads to Weight Gain

To further corroborate that it is indeed the cells of the NG2-glia class whose ablation results in the energy balance deficit, we employed mice (*Sox10-CreER*, *Esco2*$^{fl/fl}$) that were homozygous for a conditional (floxed) allele of the establishment of cohesion 1 homolog 2 gene (*Esco2)* (Whelan et al., 2012) and carried a *Sox10-iCreERT2* transgene (Simon et al., 2012). ESCO2 activity is essential for cell division and its absence causes dividing cells to die (Whelan et al., 2012), while Sox10 is a marker for oligodendrocytes (OLGs) and their precursors, i.e., NG2-glia. Tamoxifen (TX)-mediated *Cre* activation in adult *Sox10-CreER*, *Esco2*$^{fl/fl}$ mice thus produces mice that lack ESCO2 in both OLGs and NG2-glia, which consequently leads to the selective ablation of dividing NG2-glia (Figure S3D, circles), but not OLGs, as they are postmitotic (Figure S3D, hexagons). To enable assessment of NG2-glia ablation, we generated mice that additionally carried a GFP reporter allele (*Sox10-CreER*, *Esco2*$^{fl/fl}$, *GFP*).

Brains were inspected at 1 and 16 weeks post-induction of recombination (wpi) for the expression of NG2 and GFP (Figure S3D). As recombination efficacy is expected to be less then 100% (Simon et al., 2012), the total number of NG2-glia may not differ between TX-treated floxed (*Sox10-CreER*, *Esco2*$^{fl/fl}$, *GFP*) and control animals (*Sox10-CreER*, *Esco2*$^{wt/wt}$, *GFP*) at 16 wpi because non-recombined NG2-glia are expected to replace the *Esco2*-deficient NG2-glia that have been lost upon entering mitosis (Figure S3D, lower panel). Indeed, at both 1 and 16 wpi time points, hypothalamic/ME NG2-glia coverage was similar between floxed and control mice (Figures 2E–2H). However, while at 1 wpi the majority of NG2 cells were GFP+ in both groups of mice (Figures 2E and 2F, white arrows), NG2 glia were mostly GFP negative at 16 wpi in the floxed mice (Figure 2H, yellow arrows; see also schematic in Figure S3D), suggesting that ablation and replacement of *Esco2*-deficient NG2-glia has occurred. Quantitative analysis confirmed the depletion of GFP+ NG2-glia at 16 wpi with 41.56% ± 1.73% and 73.12% ± 1.61% of hypothalamic NG2-glia expressing GFP in floxed and control mice, respectively ($p < 0.0002$, unpaired t test; n = 3; mean ±SEM), with no significant difference at 1 wpi (75.75% ± 0.34% in floxed and 78.28% ± 2.09% in control mice). Concomitantly, floxed mice significantly gained weight over controls in the 16 weeks following TX treatment (Figures 2I and 2J), critically supporting our hypothesis that it is proliferating NG2-glia that are required for body weight maintenance. The body weight gain in TX-treated, floxed mice is evidently more moderate than in AraC-treated animals, as would be expected given both the lower ablation efficacy and faster replacement rate in the *Sox10-CreER*, *Esco2*$^{fl/fl}$, *GFP* model.

Central Mitotic Blockade Leads to Primary Leptin Resistance in the ArcN

Toward a mechanistic understanding of NG2-glia ablation-induced hyperphagia, we considered that obesity frequently is associated with a desensitization of hypothalamic leptin signaling (Myers et al., 2008). To assess whether leptin sensitivity is affected by NG2-glia elimination, we examined leptin-induced phosphorylation of hypothalamic signal transducer and activator of transcription 3 (STAT3) in response to leptin. We again employed AraC-mediated elimination of NG2-glia due to its high

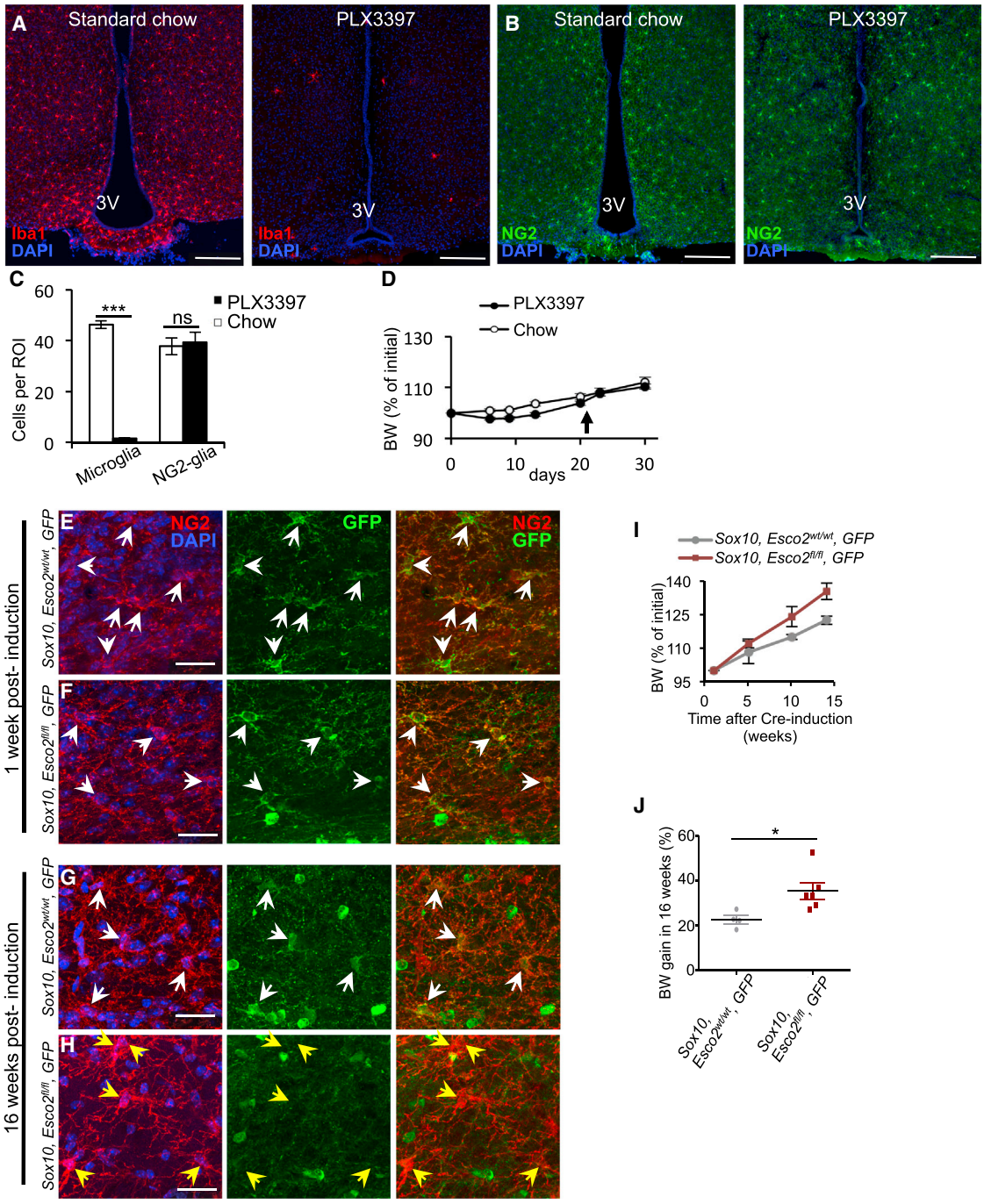

Figure 2. Genetic Ablation of Dividing NG2-Glia, but Not Total Microglia Elimination, Leads to Weight Gain

(A–D) Immunodetection of Iba-1 (A) or NG2 (B) in the mediobasal hypothalamic region of mice fed standard or PLX3397-supplemented chow and its quantitative analysis (C). (D) Body weights of mice on PLX3397 or standard chow are shown; arrow indicates return to standard chow (n = 6; ***p < 0.01, unpaired t test; ns, non-significant; Mean ± SEM). Scale bars, 200 μm.

(E and F) Immunodetection of NG2 and GFP in the hypothalamus of *Sox10*, *Esco2*$^{wt/wt}$, *GFP* (E) and *Sox10*, *Esco2*$^{fl/fl}$, *GFP* (F) mice 1 week after TX treatment. At this time point, almost all NG2-glia are GFP positive (white arrows).

(G and H) Immunodetection at 16 weeks post-TX treatment. At this time point, most NG2-glia are GFP negative in *Sox10*, *Esco2*$^{fl/fl}$, *GFP* mice (H, yellow arrows), while NG2-glia in controls (G, *Sox10*, *Esco2*$^{wt/wt}$, *GFP*) are still GFP positive (white arrows).

(I and J) Body weight gain over 16 weeks after TX treatment (I and J) in floxed (*Sox10*, *Esco2*$^{fl/fl}$, *GFP*) and control (*Sox10*, *Esco2*$^{wt/wt}$, *GFP*) mice. Dots in (J) refer to individual animals (*p < 0.05, unpaired t test; n = 4–6; mean ± SEM). Scale bars, 25 μm.

See also Figure S3.

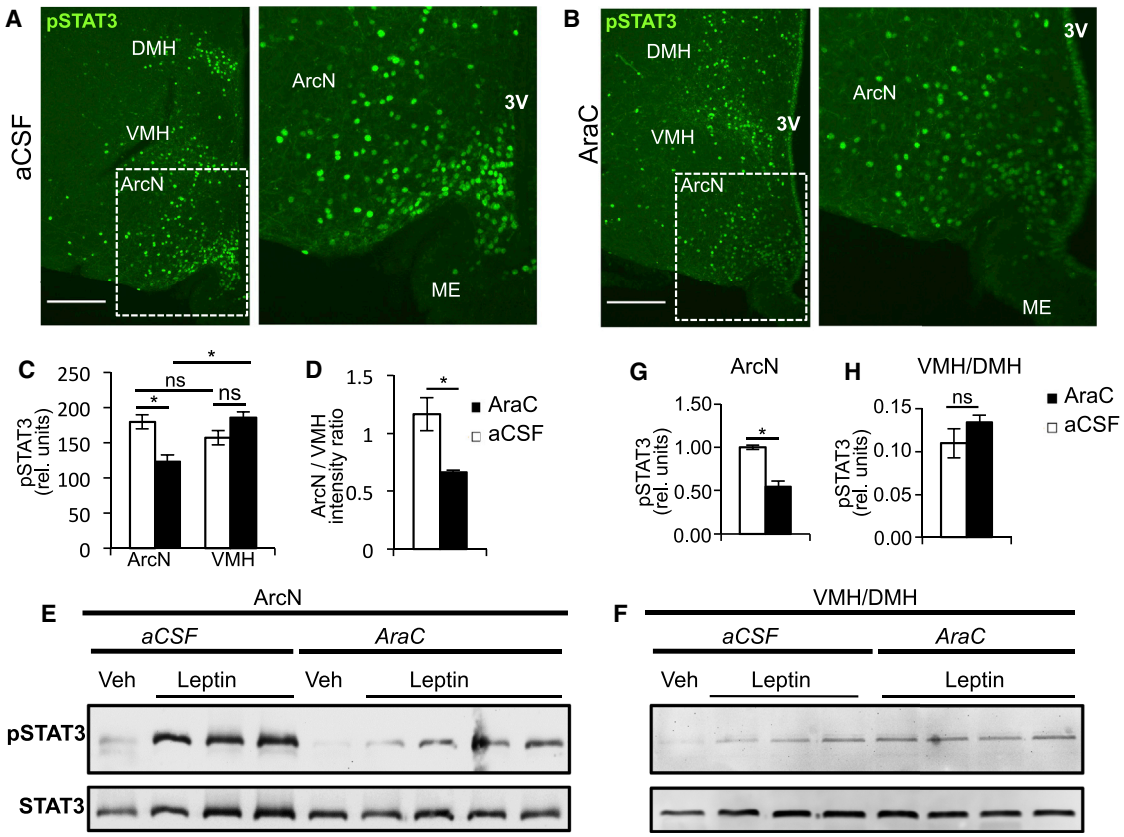

Figure 3. ArcN Leptin Signaling Is Attenuated following NG2-Glial Ablation

(A and B) Immunodetection of pSTAT3 in the mediobasal hypothalamus of aCSF- (A) or AraC- (B) infused mice 45 min after a single i.p. injection of leptin. Boxed areas (dashed lines) are shown enlarged. VMH, ventromedial nucleus; DMH, dorsomedial nucleus; 3V, third ventricle. Scale bars, 200 μm.

(C and D) Quantification of the intensity of the leptin-induced pSTAT3 immunohistochemical signal. (C) Mean fluorescence intensity of labeled somas in the ArcN and VMH is shown. (D) Ratio of mean intensities in ArcN versus VMH is shown (n = 5; unpaired t test, *p < 0.05; ns, non-significant).

(E and F) Western blot analysis of pSTAT3 induction. Protein extracts of the ArcN (E) and VMH/DMH (F) regions from aCSF- and AraC-treated animals were immunostained for pSTAT3/STAT3.

(G and H) Quantification of the western blot results for the ArcN (G) and VMH/DMH (H) regions. Shown are intensities of pSTAT3 relative to total STAT3 staining (mean ± SEM).

See also Figure S4.

ablation efficacy in the acute setting. STAT3 is an intracellular downstream component of the leptin receptor signaling pathway, and increased STAT3 phosphorylation following leptin treatment indicates leptin receptor activation (Vaisse et al., 1996). Intraperitoneal (i.p.) injections of leptin resulted in a strong, nuclear pSTAT3 staining in the ArcN and other hypothalamic feeding centers in control mice (Figure 3A), whereas AraC-infused animals showed a markedly attenuated pSTAT3 response selectively in the ArcN (Figure 3B). Quantitative analysis of immunosignal intensity confirmed these results: leptin-induced pSTAT3 in AraC-infused animals was significantly reduced in the ArcN when compared to the ventromedial nucleus (VMH) or to artificial CSF (aCSF)-infused control mice (Figures 3C and 3D). Western blot analysis further corroborated these findings (Figures 3E–3H). The leptin-induced pSTAT3-specific signal was substantially reduced in ArcN protein extracts of AraC-treated mice (Figures 3E and 3G), whereas the pSTAT3 signal in VMH/dorsomedial nucleus (DMH) extract did not differ between groups (Figures 3F and 3H). This phenotype is reminiscent of diet-induced obese (DIO) mice, which also show selective loss of leptin responsiveness in the ArcN (Münzberg et al., 2004), thought to be a consequence of the diet-induced increase in fat mass (Frederich et al., 1995).

To determine if the AraC-induced leptin resistance is similarly secondary to weight gain, we examined leptin-mediated pSTAT3 induction on day 6 of AraC infusion (Figure S4B), a time point when the excess weight gain is small but already significant (Figure S4A). Even at this early time point, the pSTAT3 response was highly blunted in the ArcN of AraC-treated mice (Figures S4C and S4D). By contrast, body weight-matched mice that were fed a high-calorie diet (HCD) until reaching similar weight gains (Figure S4A) showed only a mild attenuation of the ArcN pSTAT3 response to leptin (Figure S4E). Induction of STAT3 phosphorylation in HCD-fed animals was specific to i.p.-injected leptin, and not due to the HCD per se (Figure S4F).

Collectively, these findings indicate that NG2-glia ablation-induced leptin resistance is primary, i.e., it precedes the weight gain, suggesting a causal link.

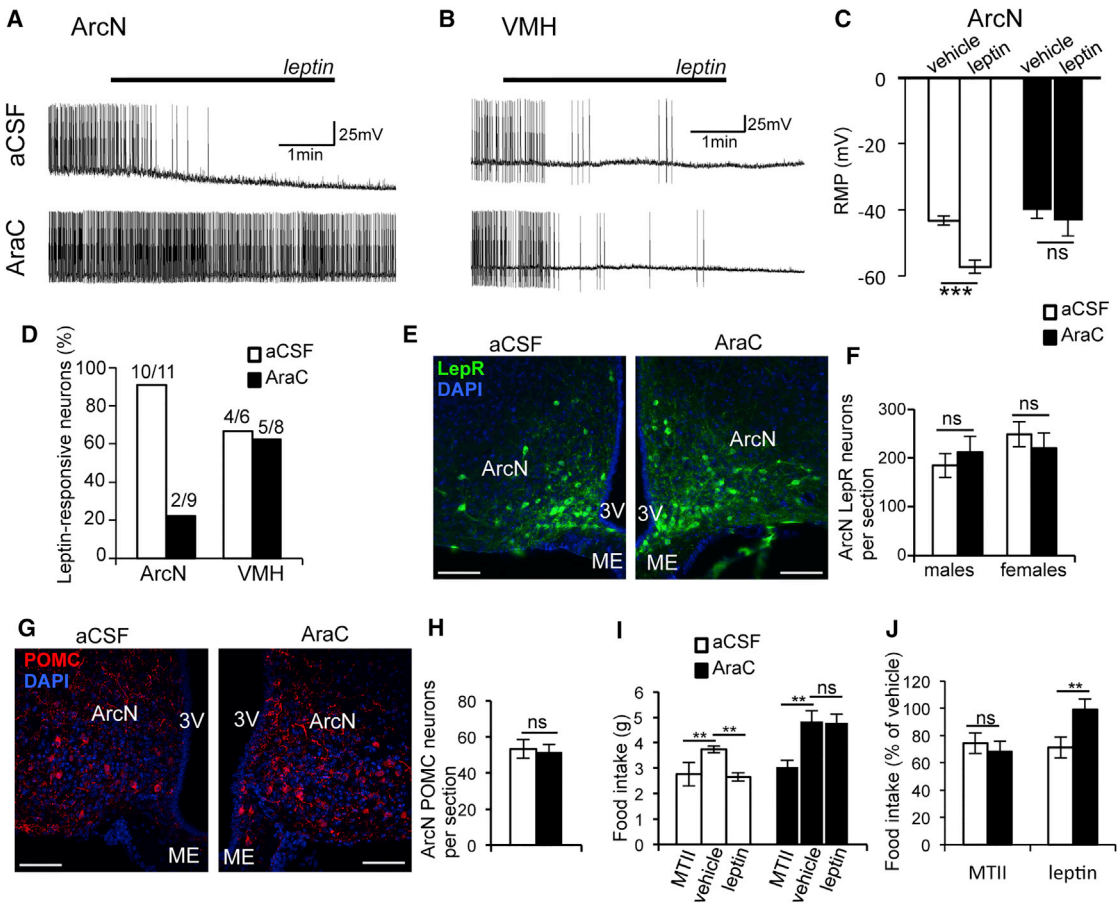

Figure 4. Electrical Responses of Hypothalamic LepR Neurons after AraC Treatment

(A–D) Patch-clamp recordings of Tom+ neurons in brain slices from *LepR-Cre* × *tdTomato* mice 1 week after termination of aCSF or AraC i.c.v. infusion. Shown are representative traces of Tom+ neurons of the ArcN (A) and VMH (B). Bars indicate the presence of 100 nM leptin in the perfusate. (C) Changes in the resting membrane potential of Tom+ neurons in response to leptin of aCSF- and AraC-treated mice (n = 9–10) are shown (***$p < 0.0001$, paired t test; ns, non–significant; mean ± SEM). (D) Percentage of neurons that showed an electrical response to exogenous leptin is indicated (for classification criteria see the Experimental Procedures).

(E–H) AraC treatment does not affect the number of LepR or POMC cells in the ArcN. GFP+ cells in the ArcN of *LepR-Cre* × *GFP* mice (E) and their quantification (F), 1 week after AraC treatment cessation, are shown. Immunodetection of POMC in the ArcN (G) and quantification of the POMC+ cell bodies (H) are shown (n = 3–4; ns, non–significant; mean ± SEM). Scale bars, 100 μm.

(I and J) Food intake of AraC-infused mice in response to i.p. leptin or MTII 2 weeks after treatment termination. Overnight food intake post-injection is displayed in grams (I) or as percentage change (J) relative to prior vehicle treatment. Mice were i.p. injected 1 hr before darkness (n = 5; **$p < 0.01$, unpaired t test; mean ± SEM).

See also Figure S5.

Loss of Electrical Responsiveness to Leptin in ArcN LepR Neurons

To further investigate the consequences of AraC treatment on ArcN LepR neuron function, we examined the electrophysiological properties of these neurons using reporter mice that express the fluorescent protein tdTomato exclusively in LepR cells (*LepR-Cre* × *tdTomato* mice). Whole-cell recordings in acute brain slices revealed no differences in the basal electrical membrane properties of tdTomato-expressing (Tom+) LepR neurons residing in the ArcN between AraC- and vehicle-infused mice (Figures S5A–S5M); thus, AraC treatment does not globally affect the electrical membrane properties or responsiveness of ArcN LepR neurons.

When leptin was added to the slice perfusate, almost all tested ArcN LepR neurons of aCSF-infused animals exhibited a marked hyperpolarization, which was associated with a loss of spontaneous firing (Figures 4A, upper trace, 4C, and 4D). This finding is consistent with the observation that GABAergic (including NPY/AgRP-positive) LepR neurons are much more numerous than glutamatergic (including POMC-positive) LepR neurons in the ArcN (Vong et al., 2011) and that only the former are expected to show hyperpolarizing responses to leptin (Cowley et al., 2001; van den Top et al., 2004).

When we next recorded from Tom+ neurons in the ArcN of AraC-infused mice, most neurons remained unresponsive (Figures 4A, lower trace, 4C, and 4D), with responsive neurons (2 of 9; Figure 4D) exhibiting only a relatively muted hyperpolarization. Leptin responsiveness of Tom+ neurons of the VMH region, on the other hand, remained unaffected by AraC treatment (Figures 4B and 4D).

AraC treatment had neither an effect on total LepR cell numbers in the ArcN (Figures 4E and 4F) nor on the number of POMC-expressing cells (Figures 4G and 4H), which are known mediators of the anorexigenic response to circulating leptin (Balthasar et al., 2004; Cowley et al., 2001). Thus, the observed weight gain is not simply due to a loss of neurons within the ArcN energy balance circuitry or a global impairment of LepR neuronal physiology, but rather due to a selective loss of leptin sensitivity in ArcN LepR neurons.

Anorexigenic Signaling Downstream of the ArcN Is Unaffected by Mitotic Blockade

If AraC-induced NG2-glia ablation indeed leads to a selective loss of leptin sensing by the ArcN circuitry, then downstream effector cells of energy balance signaling should retain normal functionality. To test this, we i.p. injected mice with the melanocortin analog MTII, which lowers food intake by activating melanocortin 4 receptor neurons of the hypothalamic paraventricular nucleus (PVN) (Marsh et al., 1999), thus mimicking the effect of endogenous α-melanocyte-stimulating hormone released by LepR-expressing POMC neurons in the ArcN (Morton et al., 2014). AraC-treated, overweight mice responded to the MTII injection with an acute reduction in food intake similarly to control animals (Figures 4I and 4J), corroborating that energy balance signaling downstream of the ArcN LepR neurons is not affected by the mitotic blocker. On the other hand, as expected, leptin treatment failed to lower food intake in AraC-treated mice (Figures 4I and 4J).

To further confirm that AraC induces primary leptin resistance, we employed *ob/ob* mice, which genetically lack endogenous leptin (Zhang et al., 1994). Despite their profound obesity, these mice are leptin sensitive, as demonstrated by their strong anorexigenic response to exogenous leptin (Pelleymounter et al., 1995). If AraC infusion indeed leads to leptin resistance independent of circulating leptin levels, then mitotic blocker would be expected to induce leptin resistance even in the complete absence of endogenous leptin. To test this, *ob/ob* mice were i.c.v. infused with AraC for 1 week, and on day 14 post-treatment cessation the animals received a single i.p. injection of leptin. We found leptin to be less effective in reducing overnight food intake in AraC- over aCSF-infused *ob/ob* mice, while i.p. MTII injections had a similar anorexigenic effect in both groups (Figures S5N and S5O). Of note, AraC treatment per se did not result in an elevation of the rate of body weight gain in *ob/ob* mice (Figure S5P), further corroborating that AraC's effect on energy balance relies solely on the impairment of leptin sensing, which is already fully absent in *ob/ob* mice.

Weight Gain Selectively Correlates with NG2-Glia Elimination from the ME and Rivals that of Leptin Signaling-Deficient Mice

In our search for the specific impairment causing the obese phenotype in AraC-treated mice, we noted that a small fraction of treated animals consistently failed to exhibit a gain in body weight in comparison to controls (Figures 5A and 5B, males; Figures S6A and S6B, females). When we then examined the extent of NG2-glia ablation on post-surgery day 7, a time when AraC-mediated cell ablation is still at its maximum and a gainer phenotype is already discernible (Figure 5C), we invariably found NG2-glia partially or fully retained in the ME in non-gainers, while gainers consistently showed a complete loss of ME NG2-glia (Figures 5D–5G). These data point to the ME as the critical site for AraC-dependent obesity induction. Notably, gainers frequently showed peak gains greater than 5 g/week, reaching body weights of up to 60 g at 8 weeks post-cannulation (Figure 5A), thereby doubling their pre-surgery body weights (also Figures S6A and S6C), which together is very reminiscent of weight gains and obesity levels seen in *ob/ob* or *db/db* mice (Coleman, 1978). These data thus suggest that complete but transient ablation of NG2-glia from the ME leads to an energy balance dysregulation, which rivals that of mice genetically lacking leptin or its receptor.

In this context it should be pointed out that the adult ME represents a particularly proliferative structure, exhibiting a 15-fold greater density of BrdU-incorporating cells when compared to the hypothalamus (Figures 5H and 5I). BrdU/NG2 co-labeling furthermore revealed that most of these cells are NG2-glia (Figure S3C), which are also more proliferative (Figure 5J) and found at much higher densities (Figure 5K) in the ME when compared to the hypothalamus proper.

To further elucidate the role of the ME NG2-glia in energy balance regulation, we considered that the ME has been proposed to mediate the anorexigenic effect of adipocyte-derived leptin (Banks et al., 1996; Faouzi et al., 2007), which is thought to exit the fenestrated portal capillary bed of the ME to activate LepR signaling in ArcN neurons (Münzberg and Morrison, 2015). To assess the anatomic basis of leptin sensing in the ME, we first inspected the ME territory for the presence of LepR neuronal processes using *LepR-Cre* × *GFP* reporter mice. Immunostaining against GFP revealed structures resembling fine processes, which frequently exhibited bead-like morphologies that appeared to traverse the ME predominantly dorsoventrally from ArcN/third ventricle to the portal capillary bed (Figures 5L, 6A, and 6B). The observed staining pattern is consistent with LepR neurons sending processes into the ME toward the fenestrated vessels to facilitate circulating leptin sensing. When we co-stained for NG2, we observed the GFP and NG2 signal in close association, with NG2-glia processes appearing to enwrap the LepR neurites (Figures 5M and 5N; Movie S1).

Mitotic Blocker Treatment Induces LepR Dendritic Process Degeneration in the ME

Next we inspected the ME of *LepR-Cre* × *GFP* mice 1 week after AraC cessation (Figures 6A–6D). To enhance the GFP signal in LepR processes, mice were stereotaxically injected into the ArcN region with the Cre-inducible *AAV-Ef1α-Flex-ArchT-GFP* virus, which potently labels neuronal processes (Amilhon et al., 2015). Compared to aCSF-infused controls (Figures 6A and 6B), which exhibit strong process-like GFP staining, the ME of AraC-treated animals showed a profound reduction in immuno-positive processes (Figures 6C and 6D). Instead, staining appeared punctate, with punctae showing a variety of sizes and shapes (Figure 6D). Such a staining pattern is reminiscent of neuronal processes undergoing degeneration/fragmentation (Kadkhodaei et al., 2013; Schaefer et al., 2007; Yun et al., 2014), suggesting that AraC-induced NG2-glia ablation causes the degradation of LepR processes in the ME. By contrast, gross LepR process architecture within the ArcN proper was

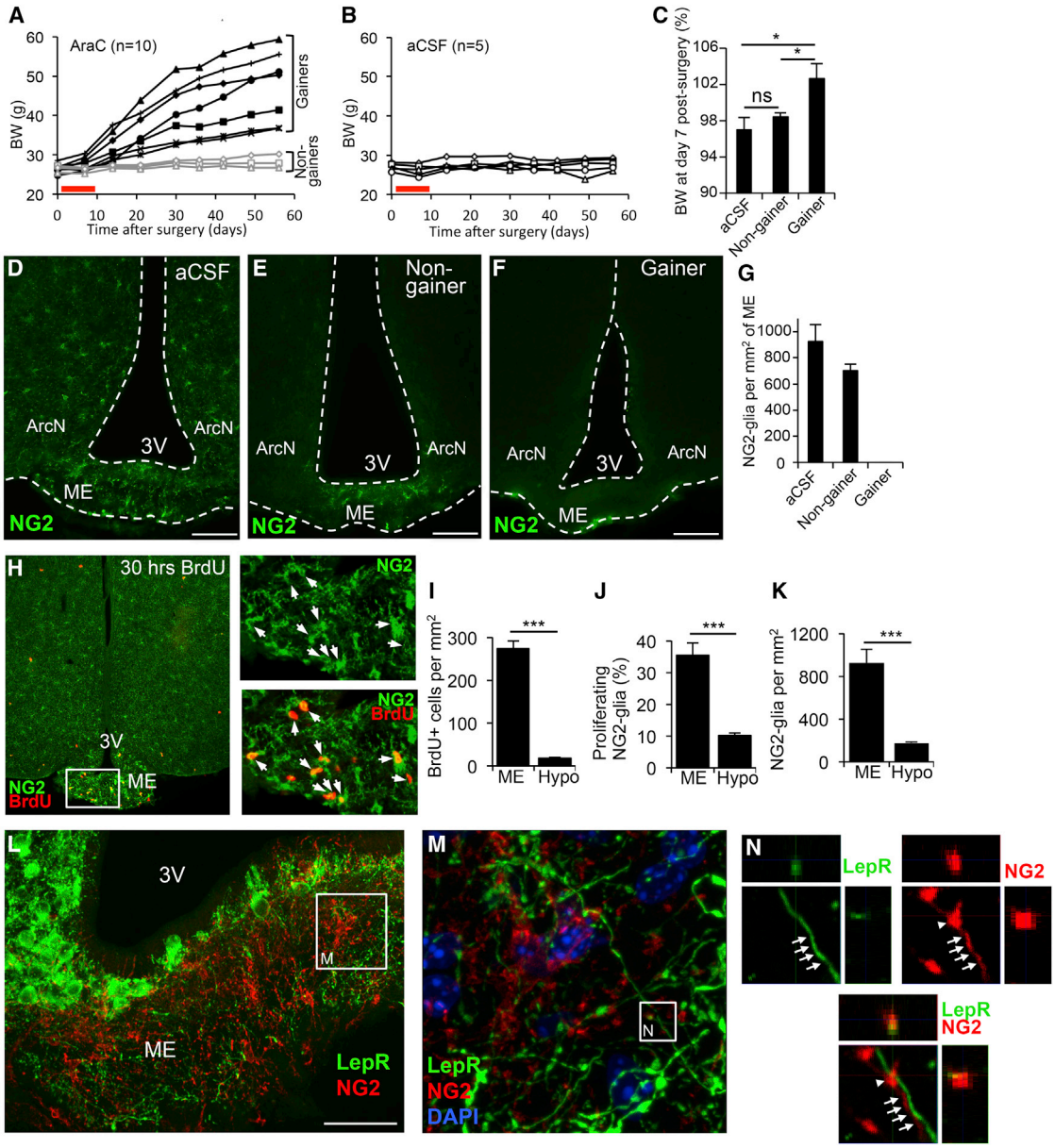

Figure 5. Correlation of ME NG2-Glia Ablation with Weight Gain

(A–C) Changes in body weights of individual male AraC- (A) and aCSF-infused (B) mice from a representative experimental cohort. Some AraC-infused animals lack the obesogenic response to AraC (gray traces). (C) Body weights on post-surgery day 7 are shown. For group classification, see Experimental Procedures (*$p < 0.05$, unpaired t test; ns, non-significant; mean ± SEM).

(D–G) Immunodetection of NG2 in the hypothalamus of aCSF- (D) and AraC-infused non-gainers (E) and gainers (F) on post-surgery day 7, during infusion. (G) Quantification of ME NG2-glia density is shown (n = 3, mean ± SEM).

(H–K) The ME shows high mitotic activity. Immunodetection of BrdU-positive NG2-glia after six BrdU i.p. injections given within 30 hr prior to sacrifice is shown. Boxed area in (H) is shown enlarged (right). Arrows indicate double-labeled cells. (I) BrdU+ cell density, (J) fraction of proliferating NG2-glia, and (K) NG2-glia density in the ME versus hypothalamic parenchyma (Hypo) are shown (***$p < 0.00001$, unpaired t test; n = 3; mean ± SEM).

(L–N) Hypothalamic sections of *LepR-Cre* × *GFP* mice immunostained for GFP and NG2. (M) is an enlargement of the boxed area in (L). (N) is the confocal orthogonal reconstruction of the area boxed in (M). Arrowhead indicates NG2 immunosignal in close apposition to a GFP+ process. Arrows mark parallel projecting NG2+/GFP+ processes.

Scale bars, 100 μm (D–F) and 50 μm (L). See also Movie S1.

indistinguishable between aCSF- and AraC-treated mice (Figures 6E and 6F).

Histochemical determination of axonal versus dendritic identity of ArcN neuronal processes by immunodetection, using markers such as neurofilament H or MAP2, was unsuccessful in our hands, in line with previous attempts on POMC (Hentges, 2007) and GnRH neurons (Herde et al., 2013). We thus resorted to immuno-electron microscopy (EM) to assess the

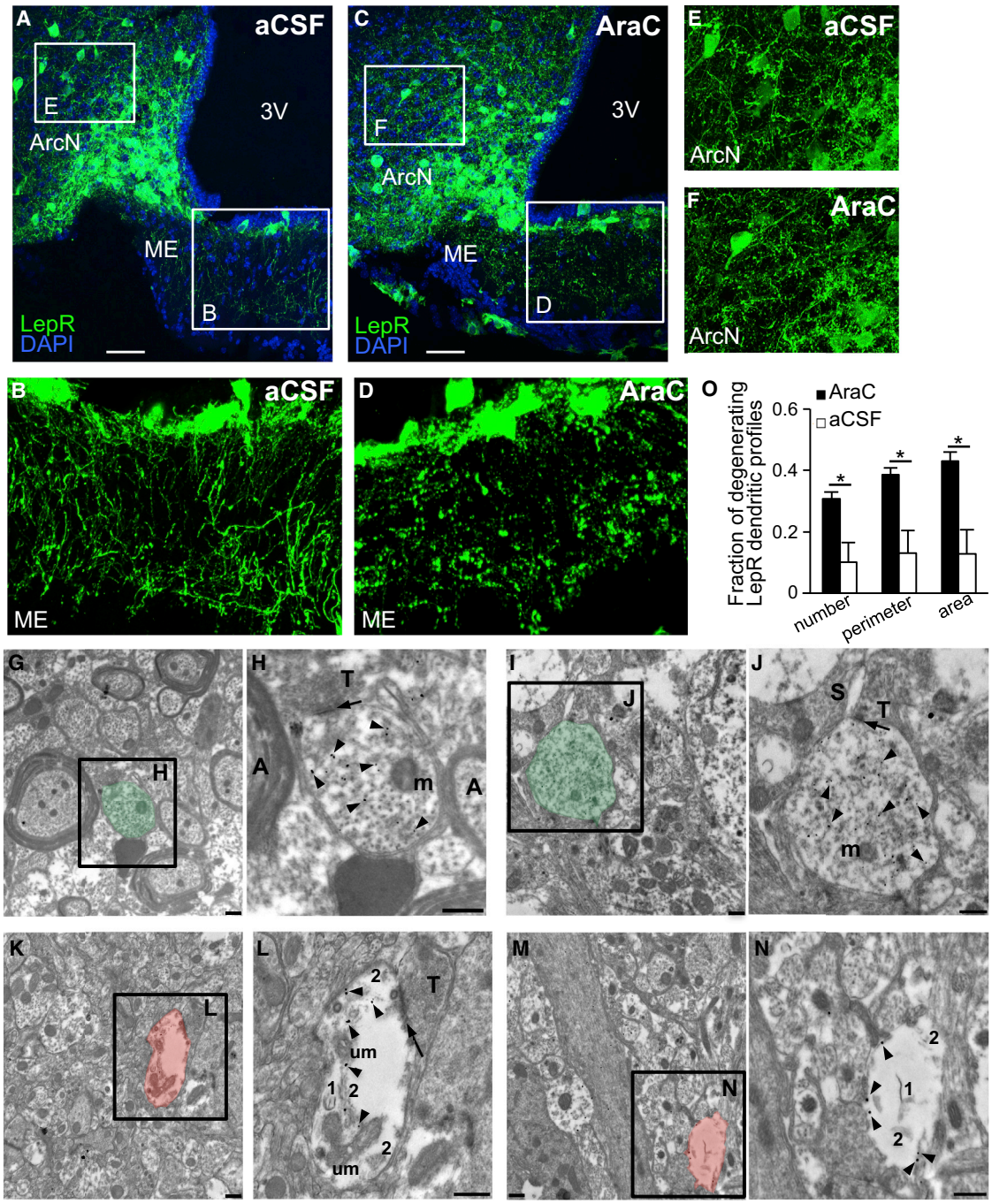

Figure 6. Morphological Assessment of ME LepR Processes in Response to AraC

(A–F) GFP immunodetection in AraC-infused, weight-gaining (C) and aCSF-infused (A) *LepR-Cre* × *GFP* mice 1 week after treatment cessation. Two weeks prior to cannula implantation, *AAVdj-Ef1α-Flex-ArchT-GFP* virus was stereotaxically injected into the ArcN to enhance process labeling. (B, D, E, and F) Enlargements of the boxed areas in (A) and (C) are shown.

(G–N) Electron micrographs of the ME from aCSF- (G–J) and AraC-infused (K–N) *LepR-Cre* × *GFP* mice 6 weeks after treatment termination. Healthy and degenerating immuno-positive dendritic profiles are highlighted in green and red, respectively. Arrowheads indicate silver-enhanced gold particles; arrows indicate postsynaptic densities. T, synaptic terminal; S, spine-like protrusion; A, axonal profile; m, healthy mitochondrion; um, unhealthy, vacuolized mitochondrion; 1, membrane whorl; 2, disintegrated organelles or cytoskeletal elements.

(O) Quantification of LepR ME dendrite degeneration at the ultrastructural level. Shown are the fraction of degenerating from total immuno-positive dendritic profiles with respect to number, perimeter, and profile area per region of interest (ROI) (n = 3; *$p < 0.05$, unpaired t test; mean ± SEM). Scale bars, 50 μm (A and C) and 500 nm (G–N).

See also Figure S6.

ultrastructural nature of the LepR processes in the ME and to further examine the degenerating effect of NG2-glia ablation on the LepR neuropil. We again employed *LepR-Cre* × *GFP* mice to enable identification of LepR processes by immuno-gold labeling against GFP (Figures 6G–6N). In aCSF-infused, *LepR-Cre* × *GFP* mice, silver-enhanced gold particles (arrowheads, Figures 6H and 6J) were found associated with profiles identified as dendrites due to the presence of postsynaptic densities (arrows, Figures 6H, 6J, and S6D–S6F), an irregular shape, and dendritic spine-like protrusions (Figures 6J, S6D, and S6E). By contrast, immuno-positive myelinated profiles or presynaptic formations were never detected, arguing against an axonal nature for the ME LepR processes. The dendritic character of the immuno-positive structures is consistent with a sensing function for the LepR processes in the ME, and it is in line with a previous finding attributing LepR expression to somato-dendritic, but not axonal, compartments of POMC and AgRP neurons (Ha et al., 2013). When we next inspected *LepR-Cre* × *GFP* mice that had gained weight in response to AraC infusion, we found many of the immuno-labeled dendritic profiles in the ME of AraC-treated animals to show signs of advanced degeneration, such as an electron-lucent cytoplasm, membrane disintegration, dark debris, and mitochondria with swollen distended cristae or holes (Figures 6K–6O). Synapses could still be observed on some of such profiles (Figure 6L, arrow), consistent with a delayed synapse loss during dendritic degeneration, as has been reported previously (Hall et al., 2000).

X-Irradiation Targeted at the ME Leads to NG2-Glia/LepR-Dendrite Loss and Weight Gain

To further confirm that mitotic blockade specifically in the ME causes a gain in body weight, we employed cranial X-irradiation, which has been used successfully to ablate NG2-glia in various brain regions (Irvine and Blakemore, 2007). Of note, there is a strong association between obesity risk and cranial X-irradiation therapy in cancer survivors. To assess the effect of X-irradiation on the ME in particular, we used lead shielding to restrict radiation exposure to the mediobasal hypothalamus/ME region. To this end, the rodent skull was surgically exposed and stereotaxically positioned so that the mediobasal hypothalamus/ME region was centered underneath a 2-mm bore in the lead shield (Figure 7A). Immunolabeling against the phosphorylated H2A histone family member X (H2AX), an indicator for ionizing radiation exposure (Rogakou et al., 1998), 1 hr after exposure to a single X-irradiation dose led to strong staining of a tissue column centered on the ME (Figures S7A–S7C), demonstrating the effectiveness of the radiation beam targeting. We next tested whether X-irradiation treatment indeed leads to NG2-glia ablation. To mark NG2-glia, we employed *NG2-CreER* × *tdTomato* mice, which first received TX to activate Tom expression selectively in NG2 cells. The mice were then X-irradiated in three sessions before receiving i.p. BrdU injections on the 3 consecutive days prior to perfusion (Figure 7B). Immunodetection of BrdU at 14 days post-irradiation revealed that the number of ME dividing cells in general, and proliferating NG2-glia in particular, was augmented over sham-treated mice (Figures 7C–7F). This result mirrors the findings of our previous AraC ablation experiments (Robins et al., 2013c), which also resulted in a net increase of BrdU+NG2+ cells post-treatment due to the replenishment of lost NG2-glia by proliferating neighboring NG2 cells. By contrast, acutely after X-irradiation treatment (3 days following the last irradiation dose), the number of NG2-glia in the ME was reduced when compared to sham-irradiated animals (Figures S7D and S7E).

Critically, we found that X-irradiation resulted in a significant increase in body weight compared to sham-irradiated controls in both males and females (Figures 7G and S7F), and this gain appears to be exclusively due to an increase in fat mass (Figure S7G). We next inspected the ME from X-irradiated mice, which had the *LepR-Cre* × *GFP* genotype, for the presence of GFP. Mice were again stereotaxically injected with *AAV-Ef1α-Flex-ArchT-GFP* into the ArcN to enhance GFP signal, 12 days prior to sacrifice. In line with our observations of AraC-treated *LepR-Cre* × *GFP* mice (see Figure 6), we detected a reduction in GFP+ process-like structures in the ME of X-irradiated, overweight mice versus mock-treated controls (Figures S7H–S7M). To quantitatively assess the extent of the process structure loss, we processed the GFP signal from individual ME images using Squassh (Rizk et al., 2014), which enables automated detection of fluorescently labeled objects (Figures S7N–S7S). While the mean object fluorescence intensity was indifferent between groups (Figure S7T), the total object surface area was decreased in the ME of irradiated mice (Figure S7U). Furthermore, even though the total number of detected objects was equivalent, the number of large objects was reduced in the ME upon irradiation (Figure S7V). This result is consistent with induction of LepR process fragmentation corresponding to our findings with AraC-treated mice.

DISCUSSION

Our data provide strong evidence that LepR neuronal processes, which reside in the ME and show hallmarks of dendrites (Figures S6D–S6F), are key to body weight control and that NG2-glia play a critical role in preserving these processes (see model, Figure 7H). We observed LepR dendritic degeneration shortly after mitotic blockade (1 week, Figures 6A–6D) but also at later time points post-AraC infusion or X-irradiation (6 weeks, Figures 6G–6O; 24 weeks, Figures S7H–S7V), suggesting that the LepR process impairment induced by short-term NG2-glia elimination is permanent. Of note, infusing AraC at a substantially lower dose of 40 μg/day (versus 120 μg/day in this study) does not lead to a weight gain (Borg et al., 2014; Kokoeva et al., 2005). We propose that this is due to low concentrations of AraC being insufficient to breach the tanycyte barrier, which is thought to isolate the ME proper from the adjacent ArcN tissue (Rodríguez et al., 2010).

The NG2-glia conceivably exert their role in process preservation by physically protecting the dendrites from the likely deleterious environment of the ME, e.g., exposure to certain blood-born substances that may freely diffuse into the ME interstitial space through the fenestrations of the ME capillaries. Alternatively or additionally, NG2-glia may provide trophic or structural support to the LepR neurites of the ME.

Interestingly, a direct involvement of glia in the maintenance of sensory dendrite integrity has been demonstrated recently for *Caenorhabditis elegans* (Bacaj et al., 2008). Here ablation of the sheath glia cell that enwraps the dendritic sensing portion

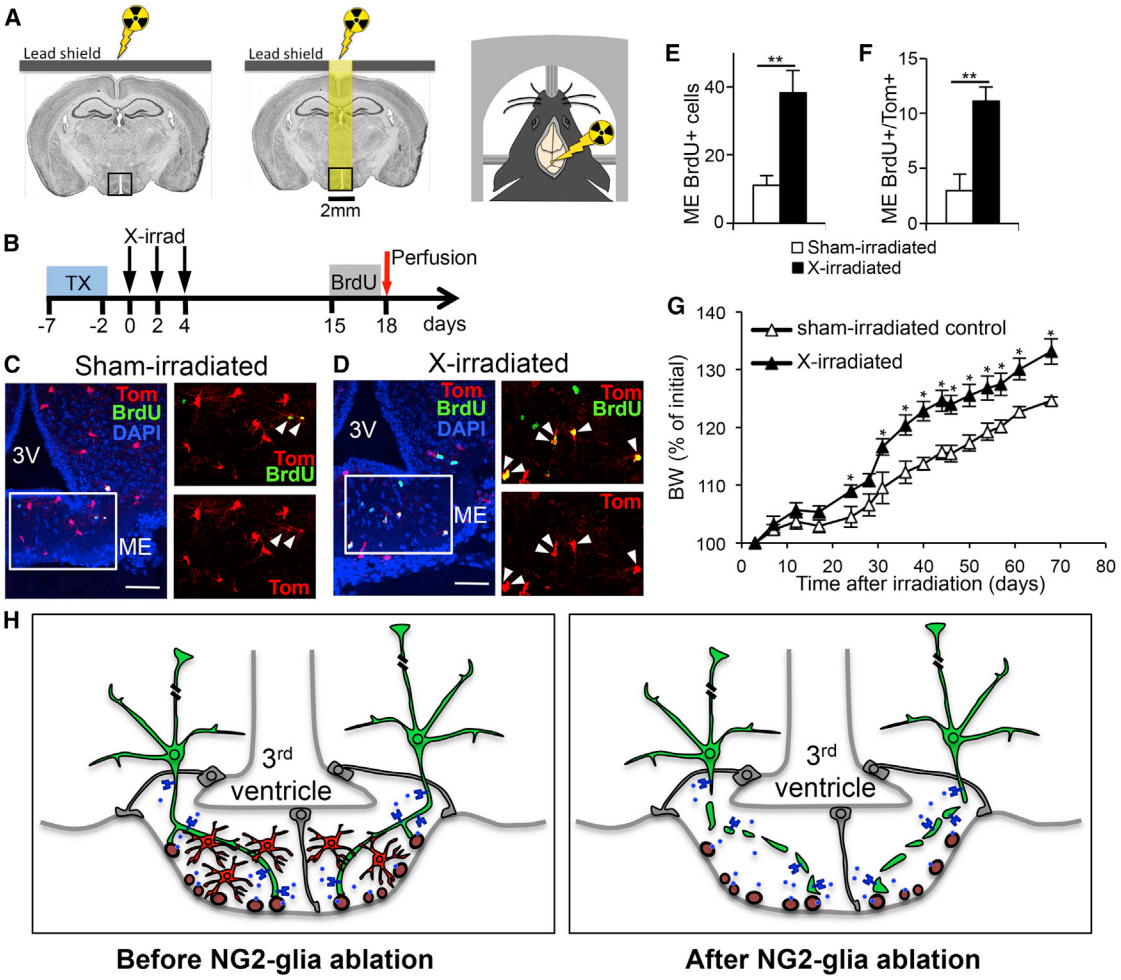

Figure 7. X-Irradiation Directed to the ME Leads to a Gain in Body Weight

(A) Illustrations depicting sham (left image) and irradiation treatment (middle image) of the ME region. For precise beam targeting and alignment, animals were stereotaxically positioned after skull exposure (right image).

(B) Treatment regimen of *NG2-CreER* × *tdTomato* mice. Animals were X-irradiated in three sessions, receiving 20 Gy per session.

(C–F) X-irradiation leads to a significant increase of BrdU+ (E) and BrdU+/Tom+ (F) cells within the ME proper (C and D) at 14 days post-irradiation treatment. Boxed areas in (C) and (D) are shown enlarged (right). Arrowheads indicate Tom+/BrdU+ cells (**$p < 0.01$, unpaired t test; n = 3–4; mean ± SEM).

(G) Body weights of sham-irradiated (n = 5) and X-irradiated (n = 10) male mice are shown (*$p < 0.05$, unpaired t test; mean ± SEM).

(H) Model of NG2-glia ablation-induced leptin resistance. Left: LepR neurons (green) extend dendritic projections past the barrier established by tanycyte processes (gray), which seal off the ArcN proper from the ME. We propose that these LepR dendrites express leptin receptors (blue) and terminate near or at fenestrated vessels (brown) of the portal capillary bed in order to sense circulating leptin (blue dots), which exits the blood vessels by passive diffusion. Right: Upon ME NG2-glia (red) ablation, LepR processes degenerate and the respective neurons lose their ability to sense leptin. This primary leptin resistance leads to overeating and obesity because other possible leptin-sensing pathways cannot compensate for the loss.

See also Figure S7.

of the chemosensory neurons in the amphid, the largest nematode sensing organ, triggers the collapse of these specialized process endings and leads to a severe blunting of the chemotactic response. Notably, glia ablation did not affect viability of these primary sensory neurons per se.

While the AraC infusion, X-irradiation, and *Esco2* disruption experiments together point to the loss of ME NG2-glia as the root cause of the observed weight gain, all three treatments also have in common a capacity to cause cell death in the ME. It could, therefore, be alternatively concluded that cell death in general, but not the particular demise of NG2-glia, leads to weight gain. If this were indeed the case, then ablation of microglia from the ME should have similar consequences, as their density seems to be comparable to that of NG2-glia in the ME (see Figures 2A, 2B, S3A, and S3B). However, total ablation of microglia from the brain parenchyma did not affect body weights, ruling out cell death per se as a trigger of the energy balance phenotype. Notably, this finding also indicates that microglia ablation does not play an important role, if any, in energy balance, at least under conditions of regular chow feeding in adult animals.

While AraC treatment led to overeating and a gain in body weight within a few days of infusion onset, the weight gain following X-irradiation focused on the ME area was much more

delayed and also milder. This discrepancy is, however, consistent with the finding that X-irradiation, in contrast to AraC treatment, leads only to a partial elimination of NG2-glia in the diencephalon, which peaks at ~2–4 weeks post-radiation treatment (Irvine and Blakemore, 2007). The incomplete ablation in case of the genetic *Esco2* disruption-based model may similarly explain its milder body weight phenotype. Irrespective of these differences, all ablation approaches lead to a weight gain over controls, strongly supporting a role for ME NG2-glia in energy balance maintenance.

Detection of circulating leptin for energy balance control previously has been associated with the ME (Faouzi et al., 2007; Myers, 2013); however, it also has been proposed that leptin sensing requires active, saturable transport across non-fenestrated brain capillaries (Banks et al., 1996; Golden et al., 1997) or uptake into the CSF by internalization of the short LepR isoform (LepRa) in the choroid plexus (Friedman, 1998). Since AraC-treated mice show an obesity phenotype that rivals that seen in mice lacking leptin or its receptor globally (Chen et al., 1996; Zhang et al., 1994), we conclude that the ME processes of LepR neurons are likely the central mediators of leptin's action on energy balance.

We do not yet know the location of the perikarya from which the ME LepR dendrites emanate. However, the selective lack of leptin responsiveness in the ArcN of AraC-treated gainers suggests that the leptin-sensing ME dendrites belong to ArcN neurons. Interestingly, an obesity phenotype resembling that of *db*/*db* or *ob*/*ob* mice also has been reported for mice that selectively lack LepR throughout the hypothalamus, including the ArcN (Ring and Zeltser, 2010), or exclusively in GABAergic neurons (Vong et al., 2011). By contrast, mice that lack LepR only in POMC neurons (Balthasar et al., 2004) or in both AgRP/NPY and POMC neurons (van de Wall et al., 2008) are only mildly overweight, although both of these ArcN neuronal populations are considered key elements of the central energy balance circuitry (Morton et al., 2014; Williams and Elmquist, 2012). The most parsimonious conclusion from these findings would then be that the ME-projecting, primary leptin-sensing neurons are likely to be GABAergic neurons residing in the ArcN, which may include AgRP/NPY neurons.

Recently, tanycytes have been implicated in leptin sensing. Leptin has been reported to be transported from the ME to the hypothalamic CSF by these specialized glia (Balland et al., 2014), which line the basal third ventricle in the mediobasal hypothalamic region with their processes contacting the ME portal capillary bed (Figure 7H). The authors reported that tanycytic processes take up leptin in the ME and then transport it to the ArcN energy balance circuits. A functional link to energy balance control was, however, not provided nor was leptin receptor expression demonstrated in tanycytes. Third-ventricular tanycytes also have been proposed to act as postnatal stem cells with the capacity for generating neurons (Lee et al., 2012; Robins et al., 2013a), and Lee et al. (2012) further implicated these cells in energy balance regulation. The authors reported that X-irradiation focused onto the ME caused a reduction in body weight and increased energy expenditure in mice, a result that is contrary to our findings. This discrepancy may be due to differences in beam characteristics or irradiation protocol and, thus, effective radiation dose at the target side.

Irradiation-associated, excessive weight gain has been specifically reported for acute lymphoblastic leukemia survivors who received cranial X-irradiation as prophylaxis against tumor recurrence (Iughetti et al., 2012). Weight gain was observed to commence during radiation treatment and obese phenotypes were sustained well beyond treatment termination. Thus, radiation therapy appears to permanently alter energy balance in these cancer survivors (Iughetti et al., 2012; Wilson et al., 2015). Of particular note, when focused radiation was employed to target distinct tumor-affected brain regions, weight gain was reported to be more substantial if the hypothalamus was within the radiation field (Lustig, 2002). Our findings now provide a potential mechanistic basis for this effect, suggesting that transient ablation of ME NG2-glia causes the weight gain.

Our data demonstrate that ME NG2-glia exhibit an exceptionally high degree of turnover when compared to the hypothalamic parenchyma and perhaps most other brain sites. They are five times denser and 3.5 times more mitotically active than elsewhere in the hypothalamus. This may explain why NG2-glia ablation has such dramatic consequences on energy balance regulation, but not other ME-independent hypothalamic functions. The high ME NG2-glia turnover might be owing to the fact that the ME represents an extra-brain structure providing a particularly challenging environment for NG2-glia and/or neuropil. These observations lend support to the idea that the ME LepR neurite/NG2-glia ensemble represents an Achilles' heel of energy balance regulation, whose impairment can permanently and profoundly alter body weight set levels.

EXPERIMENTAL PROCEDURES

Animals

Mice were housed under a 12-hr light:12-hr dark cycle with lights on at 7 a.m., and experiments were performed on 8- to 12-week-old mice of either sex, if not otherwise noted. All animal procedures were carried out in accordance with the recommendations of the Canadian Council on Animal Care (CCAC), and they have been approved by the McGill University Animal Care Committee.

Diets

Mice were fed regular chow (2018s, Harlan Laboratories) or high-calorie chow (D12492, Research Diets) for obesity induction. To ablate microglia from the brain parenchyma, mice were fed a chow diet supplemented with the CSF1R inhibitor PLX3397 (290 mg/kg, Plexikkon).

AraC Treatment and Weight Gain Phenotype Classification

AraC (Sigma) was administered via osmotic minipumps (flow rate 0.5 μL/hr, 7-day pumps, Alzet) as previously described (Robins et al., 2013c). AraC was infused in aCSF at a dose of 120 μg/day while control mice received aCSF alone. Mice were anesthetized with a ketamine (100 mg/kg)/xylazine (10 mg/kg) cocktail (KX) in preparation for surgery. They were stereotaxically (Kopf Instruments) implanted with a steel cannula (328OPM/Spc, Plastics One) into the right lateral ventricle (anteroposterior −0.3 mm, lateral +1.0 mm to bregma, and dorsoventral −2.6 mm below skull). Alternatively, cannulae were lowered into the third (stereotaxic coordinates −1.7 mm anteroposterior, 0 mm lateral, and −5.94 mm dorsoventral) or fourth (stereotaxic coordinates −6.0 mm anteroposterior, 0 mm lateral, and −4.1 mm dorsoventral) ventricular spaces. The tubing (Plastics One, inner diameter 0.69 mm) connecting the pump to the cannula was cut to a length of 67 mm and filled with aCSF. This allowed for a recovery period of 48 hr following surgery, during which mice received only aCSF. Based on retrospective analysis on AraC-treated mice that were monitored long term, body weight phenotypes were determined as follows for day 7 post-cannulation surgery: mice that had gained more

than two SDs above the mean body weight of vehicle-infused controls were considered gainers, whereas mice that had gained less than one SD above the mean were considered non-gainers.

X-Irradiation of the Hypothalamus/ME Region

Mice were stereotaxically positioned to align the ME/mediobasal hypothalamus with the 2-mm bore drilled through the custom-made lead shield covering the animal's skull and body. The shielded mouse was then placed into an X-irradiator (Rad Source 2000 Biological Research Irradiator), and mice were irradiated in three sessions receiving a total of 45 or 60 Gy.

Leptin/MTII Treatment

Leptin (National Hormone and Peptide Program) or MTII (Bachem) was dissolved in 1× PBS. For assessing pSTAT3 induction, fasted mice were given a single i.p. injection 1 hr prior to perfusion with a leptin dose of 7.5 μg/g body weight. For assessing the effect of exogenous leptin and MTII on overnight food intake, mice were i.p. injected with leptin (2.5 μg/g body weight) or MTII (4 μg/g body weight) 1 hr before lights off, and subsequent food intake was measured 16 hr later (3 hr after lights on).

Statistical Analysis

Group data are presented as mean ± SEM. Statistical significance was calculated using paired or unpaired two-tailed Student's t test, except for the Squaash3C analysis, where a two-way ANOVA was applied. If not otherwise noted, statistical significance was indicated as follows: *$p < 0.05$, **$p < 0.01$, and ***$p < 0.001$; ns, non-significant.

SUPPLEMENTAL INFORMATION

Supplemental Information includes Supplemental Experimental Procedures, seven figures, and one movie and can be found with this article online at http://dx.doi.org/10.1016/j.cmet.2016.04.013.

AUTHOR CONTRIBUTIONS

M.V.K., T.D., S.C.R., and L.D. designed the experiments. T.D., S.C.R., S.S., D.K., C.J.G., A.M., X.L., and J.H.K. conducted the experiments. Experiments were assisted by contributions from T.S., C.W.B., K.-F.S., and U.B. All authors contributed to discussions about the data and their interpretation. M.V.K., S.C.R., and T.D. wrote the manuscript.

ACKNOWLEDGMENTS

We thank Gregor Eichele for providing us with the *Esco2*$^{fl/fl}$ mouse line, Christopher Law for assistance with automated image analysis, Walter Kucharski for manufacturing the customized lead shield for the irradiation experiments, and Alan Peterson for helpful comments on the manuscript. We are grateful to Min Fu and the Molecular Imaging Platform at the Research Institute of the McGill University Health Center for assistance with confocal microcopy. We also thank Edward Boyden for the viral construct and Aurélien Rizk and Philipp Berger for aiding us in the use of the Squassh3C software. This work was supported by Canadian Institutes of Health Research operating grants MOP-102511 to M.V.K., MOP-E-201759 to K.-F.S., and FDN-143337 to C.W.B. Financial support for L.D. was provided by the SFB 870, the SPP1757 of the Deutsche Forschungsgemeinschaft, the ERA-NET (NEURON) project supported by the Bundesministerium für Bildung und Forschung (BMBF), the Excellence Initiative Synergy, and the Friedrich Bauer Stiftung.

Received: December 1, 2015
Revised: February 12, 2016
Accepted: April 13, 2016
Published: May 10, 2016

REFERENCES

Amilhon, B., Huh, C.Y., Manseau, F., Ducharme, G., Nichol, H., Adamantidis, A., and Williams, S. (2015). Parvalbumin Interneurons of Hippocampus Tune Population Activity at Theta Frequency. Neuron *86*, 1277–1289.

Bacaj, T., Tevlin, M., Lu, Y., and Shaham, S. (2008). Glia are essential for sensory organ function in C. elegans. Science *322*, 744–747.

Balland, E., Dam, J., Langlet, F., Caron, E., Steculorum, S., Messina, A., Rasika, S., Falluel-Morel, A., Anouar, Y., Dehouck, B., et al. (2014). Hypothalamic tanycytes are an ERK-gated conduit for leptin into the brain. Cell Metab. *19*, 293–301.

Balthasar, N., Coppari, R., McMinn, J., Liu, S.M., Lee, C.E., Tang, V., Kenny, C.D., McGovern, R.A., Chua, S.C., Jr., Elmquist, J.K., and Lowell, B.B. (2004). Leptin receptor signaling in POMC neurons is required for normal body weight homeostasis. Neuron *42*, 983–991.

Banks, W.A., Kastin, A.J., Huang, W., Jaspan, J.B., and Maness, L.M. (1996). Leptin enters the brain by a saturable system independent of insulin. Peptides *17*, 305–311.

Becker, E.E., and Grinker, J.A. (1977). Meal patterns in the genetically obese Zucker rat. Physiol. Behav. *18*, 685–692.

Bergles, D.E., Roberts, J.D., Somogyi, P., and Jahr, C.E. (2000). Glutamatergic synapses on oligodendrocyte precursor cells in the hippocampus. Nature *405*, 187–191.

Borg, M.L., Lemus, M., Reichenbach, A., Selathurai, A., Oldfield, B.J., Andrews, Z.B., and Watt, M.J. (2014). Hypothalamic neurogenesis is not required for the improved insulin sensitivity following exercise training. Diabetes *63*, 3647–3658.

Chen, H., Charlat, O., Tartaglia, L.A., Woolf, E.A., Weng, X., Ellis, S.J., Lakey, N.D., Culpepper, J., Moore, K.J., Breitbart, R.E., et al. (1996). Evidence that the diabetes gene encodes the leptin receptor: identification of a mutation in the leptin receptor gene in db/db mice. Cell *84*, 491–495.

Coleman, D.L. (1978). Obese and diabetes: two mutant genes causing diabetes-obesity syndromes in mice. Diabetologia *14*, 141–148.

Cowley, M.A., Smart, J.L., Rubinstein, M., Cerdán, M.G., Diano, S., Horvath, T.L., Cone, R.D., and Low, M.J. (2001). Leptin activates anorexigenic POMC neurons through a neural network in the arcuate nucleus. Nature *411*, 480–484.

De Biase, L.M., Nishiyama, A., and Bergles, D.E. (2010). Excitability and synaptic communication within the oligodendrocyte lineage. J. Neurosci. *30*, 3600–3611.

Dimou, L., and Gallo, V. (2015). NG2-glia and their functions in the central nervous system. Glia *63*, 1429–1451.

Elmore, M.R., Najafi, A.R., Koike, M.A., Dagher, N.N., Spangenberg, E.E., Rice, R.A., Kitazawa, M., Matusow, B., Nguyen, H., West, B.L., and Green, K.N. (2014). Colony-stimulating factor 1 receptor signaling is necessary for microglia viability, unmasking a microglia progenitor cell in the adult brain. Neuron *82*, 380–397.

Faouzi, M., Leshan, R., Björnholm, M., Hennessey, T., Jones, J., and Münzberg, H. (2007). Differential accessibility of circulating leptin to individual hypothalamic sites. Endocrinology *148*, 5414–5423.

Frederich, R.C., Hamann, A., Anderson, S., Löllmann, B., Lowell, B.B., and Flier, J.S. (1995). Leptin levels reflect body lipid content in mice: evidence for diet-induced resistance to leptin action. Nat. Med. *1*, 1311–1314.

Friedman, J.M. (1998). Leptin, leptin receptors, and the control of body weight. Nutr. Rev. *56*, s38–s46.

Gao, Y., Ottaway, N., Schriever, S.C., Legutko, B., García-Cáceres, C., de la Fuente, E., Mergen, C., Bour, S., Thaler, J.P., Seeley, R.J., et al. (2014). Hormones and diet, but not body weight, control hypothalamic microglial activity. Glia *62*, 17–25.

García-Cáceres, C., Yi, C.X., and Tschöp, M.H. (2013). Hypothalamic astrocytes in obesity. Endocrinol. Metab. Clin. North Am. *42*, 57–66.

Gibson, E.M., Purger, D., Mount, C.W., Goldstein, A.K., Lin, G.L., Wood, L.S., Inema, I., Miller, S.E., Bieri, G., Zuchero, J.B., et al. (2014). Neuronal activity promotes oligodendrogenesis and adaptive myelination in the mammalian brain. Science *344*, 1252304.

Golden, P.L., Maccagnan, T.J., and Pardridge, W.M. (1997). Human blood-brain barrier leptin receptor. Binding and endocytosis in isolated human brain microvessels. J. Clin. Invest. *99*, 14–18.

Ha, S., Baver, S., Huo, L., Gata, A., Hairston, J., Huntoon, N., Li, W., Zhang, T., Benecchi, E.J., Ericsson, M., et al. (2013). Somato-dendritic localization and

signaling by leptin receptors in hypothalamic POMC and AgRP neurons. PLoS ONE *8*, e77622.

Hall, G.F., Chu, B., Lee, G., and Yao, J. (2000). Human tau filaments induce microtubule and synapse loss in an in vivo model of neurofibrillary degenerative disease. J. Cell Sci. *113*, 1373–1387.

Hentges, S.T. (2007). Synaptic regulation of proopiomelanocortin neurons can occur distal to the arcuate nucleus. J. Neurophysiol. *97*, 3298–3304.

Herde, M.K., Iremonger, K.J., Constantin, S., and Herbison, A.E. (2013). GnRH neurons elaborate a long-range projection with shared axonal and dendritic functions. J. Neurosci. *33*, 12689–12697.

Ho, A., and Chin, A. (1988). Circadian feeding and drinking patterns of genetically obese mice fed solid chow diet. Physiol. Behav. *43*, 651–656.

Hughes, E.G., Kang, S.H., Fukaya, M., and Bergles, D.E. (2013). Oligodendrocyte progenitors balance growth with self-repulsion to achieve homeostasis in the adult brain. Nat. Neurosci. *16*, 668–676.

Irvine, K.A., and Blakemore, W.F. (2007). A different regional response by mouse oligodendrocyte progenitor cells (OPCs) to high-dose X-irradiation has consequences for repopulating OPC-depleted normal tissue. Eur. J. Neurosci. *25*, 417–424.

Iughetti, L., Bruzzi, P., Predieri, B., and Paolucci, P. (2012). Obesity in patients with acute lymphoblastic leukemia in childhood. Ital. J. Pediatr. *38*, 4.

Kadkhodaei, B., Alvarsson, A., Schintu, N., Ramsköld, D., Volakakis, N., Joodmardi, E., Yoshitake, T., Kehr, J., Decressac, M., Björklund, A., et al. (2013). Transcription factor Nurr1 maintains fiber integrity and nuclear-encoded mitochondrial gene expression in dopamine neurons. Proc. Natl. Acad. Sci. USA *110*, 2360–2365.

Kokoeva, M.V., Yin, H., and Flier, J.S. (2005). Neurogenesis in the hypothalamus of adult mice: potential role in energy balance. Science *310*, 679–683.

Kokoeva, M.V., Yin, H., and Flier, J.S. (2007). Evidence for constitutive neural cell proliferation in the adult murine hypothalamus. J. Comp. Neurol. *505*, 209–220.

Lee, D.A., Bedont, J.L., Pak, T., Wang, H., Song, J., Miranda-Angulo, A., Takiar, V., Charubhumi, V., Balordi, F., Takebayashi, H., et al. (2012). Tanycytes of the hypothalamic median eminence form a diet-responsive neurogenic niche. Nat. Neurosci. *15*, 700–702.

Lustig, R.H. (2002). Hypothalamic obesity: the sixth cranial endocrinopathy. Endocrinologist *12*, 210–217.

Marsh, D.J., Hollopeter, G., Huszar, D., Laufer, R., Yagaloff, K.A., Fisher, S.L., Burn, P., and Palmiter, R.D. (1999). Response of melanocortin-4 receptor-deficient mice to anorectic and orexigenic peptides. Nat. Genet. *21*, 119–122.

McKenzie, I.A., Ohayon, D., Li, H., de Faria, J.P., Emery, B., Tohyama, K., and Richardson, W.D. (2014). Motor skill learning requires active central myelination. Science *346*, 318–322.

Morton, G.J., Meek, T.H., and Schwartz, M.W. (2014). Neurobiology of food intake in health and disease. Nat. Rev. Neurosci. *15*, 367–378.

Münzberg, H., and Morrison, C.D. (2015). Structure, production and signaling of leptin. Metabolism *64*, 13–23.

Münzberg, H., Flier, J.S., and Bjørbaek, C. (2004). Region-specific leptin resistance within the hypothalamus of diet-induced obese mice. Endocrinology *145*, 4880–4889.

Myers, M.G., Jr. (2013). How is the hungry brain like a sieve? Cell Metab. *17*, 467–468.

Myers, M.G., Cowley, M.A., and Münzberg, H. (2008). Mechanisms of leptin action and leptin resistance. Annu. Rev. Physiol. *70*, 537–556.

Pelleymounter, M.A., Cullen, M.J., Baker, M.B., Hecht, R., Winters, D., Boone, T., and Collins, F. (1995). Effects of the obese gene product on body weight regulation in ob/ob mice. Science *269*, 540–543.

Ring, L.E., and Zeltser, L.M. (2010). Disruption of hypothalamic leptin signaling in mice leads to early-onset obesity, but physiological adaptations in mature animals stabilize adiposity levels. J. Clin. Invest. *120*, 2931–2941.

Rizk, A., Paul, G., Incardona, P., Bugarski, M., Mansouri, M., Niemann, A., Ziegler, U., Berger, P., and Sbalzarini, I.F. (2014). Segmentation and quantification of subcellular structures in fluorescence microscopy images using Squassh. Nat. Protoc. *9*, 586–596.

Robins, S.C., Stewart, I., McNay, D.E., Taylor, V., Giachino, C., Goetz, M., Ninkovic, J., Briancon, N., Maratos-Flier, E., Flier, J.S., et al. (2013a). α-Tanycytes of the adult hypothalamic third ventricle include distinct populations of FGF-responsive neural progenitors. Nat. Commun. *4*, 2049.

Robins, S.C., Trudel, E., Rotondi, O., Liu, X., Djogo, T., Kryzskaya, D., Bourque, C.W., and Kokoeva, M.V. (2013b). Evidence for NG2-glia derived, adult-born functional neurons in the hypothalamus. PLoS ONE *8*, e78236.

Robins, S.C., Villemain, A., Liu, X., Djogo, T., Kryzskaya, D., Storch, K.F., and Kokoeva, M.V. (2013c). Extensive regenerative plasticity among adult NG2-glia populations is exclusively based on self-renewal. Glia *61*, 1735–1747.

Rodríguez, E.M., Blázquez, J.L., and Guerra, M. (2010). The design of barriers in the hypothalamus allows the median eminence and the arcuate nucleus to enjoy private milieus: the former opens to the portal blood and the latter to the cerebrospinal fluid. Peptides *31*, 757–776.

Rogakou, E.P., Pilch, D.R., Orr, A.H., Ivanova, V.S., and Bonner, W.M. (1998). DNA double-stranded breaks induce histone H2AX phosphorylation on serine 139. J. Biol. Chem. *273*, 5858–5868.

Schaefer, A., O'Carroll, D., Tan, C.L., Hillman, D., Sugimori, M., Llinas, R., and Greengard, P. (2007). Cerebellar neurodegeneration in the absence of microRNAs. J. Exp. Med. *204*, 1553–1558.

Simon, C., Lickert, H., Götz, M., and Dimou, L. (2012). Sox10-iCreERT2 : a mouse line to inducibly trace the neural crest and oligodendrocyte lineage. Genesis *50*, 506–515.

Thaler, J.P., Yi, C.X., Schur, E.A., Guyenet, S.J., Hwang, B.H., Dietrich, M.O., Zhao, X., Sarruf, D.A., Izgur, V., Maravilla, K.R., et al. (2012). Obesity is associated with hypothalamic injury in rodents and humans. J. Clin. Invest. *122*, 153–162.

Vaisse, C., Halaas, J.L., Horvath, C.M., Darnell, J.E., Jr., Stoffel, M., and Friedman, J.M. (1996). Leptin activation of Stat3 in the hypothalamus of wild-type and ob/ob mice but not db/db mice. Nat. Genet. *14*, 95–97.

van de Wall, E., Leshan, R., Xu, A.W., Balthasar, N., Coppari, R., Liu, S.M., Jo, Y.H., MacKenzie, R.G., Allison, D.B., Dun, N.J., et al. (2008). Collective and individual functions of leptin receptor modulated neurons controlling metabolism and ingestion. Endocrinology *149*, 1773–1785.

van den Top, M., Lee, K., Whyment, A.D., Blanks, A.M., and Spanswick, D. (2004). Orexigen-sensitive NPY/AgRP pacemaker neurons in the hypothalamic arcuate nucleus. Nat. Neurosci. *7*, 493–494.

Vong, L., Ye, C., Yang, Z., Choi, B., Chua, S., Jr., and Lowell, B.B. (2011). Leptin action on GABAergic neurons prevents obesity and reduces inhibitory tone to POMC neurons. Neuron *71*, 142–154.

Whelan, G., Kreidl, E., Wutz, G., Egner, A., Peters, J.M., and Eichele, G. (2012). Cohesin acetyltransferase Esco2 is a cell viability factor and is required for cohesion in pericentric heterochromatin. EMBO J. *31*, 71–82.

Williams, K.W., and Elmquist, J.K. (2012). From neuroanatomy to behavior: central integration of peripheral signals regulating feeding behavior. Nat. Neurosci. *15*, 1350–1355.

Wilson, C.L., Liu, W., Yang, J.J., Kang, G., Ojha, R.P., Neale, G.A., Srivastava, D.K., Gurney, J.G., Hudson, M.M., Robison, L.L., and Ness, K.K. (2015). Genetic and clinical factors associated with obesity among adult survivors of childhood cancer: a report from the St. Jude Lifetime Cohort. Cancer *121*, 2262–2270.

Young, K.M., Psachoulia, K., Tripathi, R.B., Dunn, S.J., Cossell, L., Attwell, D., Tohyama, K., and Richardson, W.D. (2013). Oligodendrocyte dynamics in the healthy adult CNS: evidence for myelin remodeling. Neuron *77*, 873–885.

Yun, J., Puri, R., Yang, H., Lizzio, M.A., Wu, C., Sheng, Z.H., and Guo, M. (2014). MUL1 acts in parallel to the PINK1/parkin pathway in regulating mitofusin and compensates for loss of PINK1/parkin. eLife *3*, e01958.

Zhang, Y., Proenca, R., Maffei, M., Barone, M., Leopold, L., and Friedman, J.M. (1994). Positional cloning of the mouse obese gene and its human homologue. Nature *372*, 425–432.